A Fully Integrated RF-Powered Contact Lens With a Single Element Display

Jagdish Pandey, *Student Member, IEEE*, Yu-Te Liao, *Student Member, IEEE*, Andrew Lingley, Ramin Mirjalili, Babak Parviz, and Brian P. Otis, *Senior Member, IEEE*

***Abstract*—We present progress toward a wirelessly-powered active contact lens comprised of a transparent polymer substrate, loop antenna, power harvesting IC, and micro-LED. The fully integrated radio power harvesting and power management system was fabricated in a $0.13\ \mu\mathrm{m}$ CMOS process with a total die area of $0.2\ \mathrm{mm}^2$. It utilizes a small on-chip capacitor for energy storage to light up a micro-LED pixel. We have demonstrated wireless power transfer at 10 cm distance using the custom IC and on-lens antenna.**

***Index Terms*—Energy harvesting, flip chip, lens, low-power electronics, optical device fabrication, power management, rectennas, rectifier.**

I. Introduction

CONVENTIONAL contact lenses are transparent polymers placed on the eye to correct faulty vision. There are two primary avenues through which contacts lens functionality could be expanded by creating heterogeneous systems with embedded electronics.

First, contact lenses could be used as a platform on which to build a display. Such a device could be remotely powered, communicate with a PDA or cell phone, and continuously provide the user with pertinent information. A lens with a single pixel could aid those with impaired hearing or could be incorporated as an indicator into video games. With more colors and higher resolution, lens functionality could be expanded to display text or offer visual cues from a navigation system [1].

Second, an active contact lens could make use of its local environment to monitor wearer's health. Tear fluid contains many biomarkers that closely correlate to levels found in blood, such as glucose, cholersterol, sodium, and potassium [2]. Thus, through integrating biological sensors and telemetry, an active contact lens could provide health professionals with a new tool for research studies and for diagnosing diseases, without the need for lab chemistry or needles [3]. Fig. 1 shows a conceptual diagram of an active contact lens.

Prior work [4]–[6] on active lens has primarily focused on developing an embedded sensor on a contact lens for medical monitoring. Also, to the best of authors' knowledge, none have demonstrated a fully autonomous integrated system on lens using RF power. For example, Leonardi *et al.* [4] demonstrated an embedded MEMS strain gauge sensor on a contact lens for measuring intraocular pressure [4]. However, the device does not incorporate a telemetry chip and the sensor readout interface involves wired connection to the lens. In [5], the single chip intraocular pressure sensor implanted in the eye's lens is powered using a 13.56 MHz inductive link with the external unit embedded in spectacle frame. Inductive links offer a relatively short range of operation and the external reader unit needs to be mounted close to the eye. Cong *et al.* [6] realized a capacitive pressure sensor on lens but do not implement a read-out circuitry. In [7], a wirelessly powered LED display and a driver chip was created to project an image onto the retina. However, the display was implanted into the ocular lens to restore vision lost due to opaque cornea, whereas this work focuses on developing a display contained within a contact lens for those with normal vision. Additionally, the details of wireless energy transfer are not provided.

In summary, neither the display functionality nor the RF-powered lens has been attempted before to the best of our knowledge. In this work, we focus on incorporating a fully integrated, elementary display functionality on to a contact lens using far-field energy harvesting. Specifically, we present progress toward a single pixel display consisting of a micro-LED, a far-field 2.4 GHz wireless energy harvesting and energy management chip, and on-lens loop antenna.

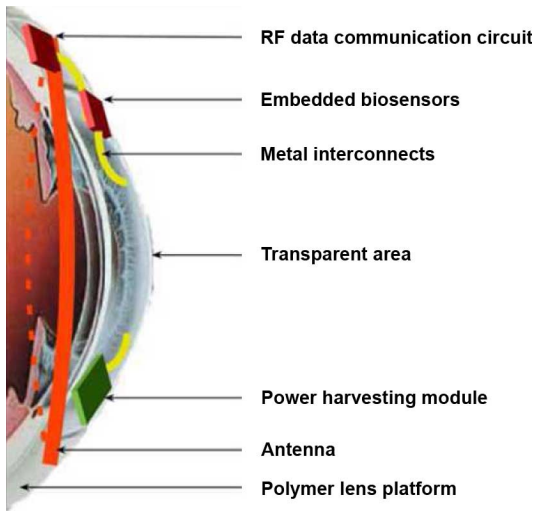

Fig. 1. A conceptual drawing of an active contact lens.

Manuscript received May 15, 2010; revised August 08, 2010; accepted September 21, 2010. Date of publication November 09, 2010; date of current version November 24, 2010. This work was supported in part by Microsoft, in part by the National Science Foundation, and in part by the UW Technology Gap Innovation Fund. This paper was recommended by Associate Editor A. Bermak.

The authors are with the Department of Electrical Engineering, University of Washington, Seattle, WA 98195 USA (e-mail: jnpandey@uw.edu; yudo@u.washington.edu; alingley@u.washington.edu; ramin@u.washington.edu; parviz@u.washington.edu; botis@u.washington.edu).

Color versions of one or more of the figures in this paper are available online at http://ieeexplore.ieee.org.

Digital Object Identifier 10.1109/TBCAS.2010.2081989

There are four main challenges in developing such a contact lens. First, sufficient energy must be available to power the sensors, display, and communication circuitry. Environmental photovoltaic generation from the sun or fluorescent lighting may be appropriate for sensing, where power requirements are very low. We chose radio frequency power to provide sufficient energy for wireless operation of a single-pixel display.

Secondly, the lens system must meet biocompatibility requirements. This applies to the contact lens platform and its constituent components, which could include display elements, integrated circuits, antennas, and sensors. For example, red LEDs made of toxic aluminum gallium arsenide must be enveloped in a biocompatible substance for safe operation. Additionally, safety standards place limits on incident radio frequency radiation. Therefore, the energy efficiency of the electrical and optical subcomponents is of utmost importance. In order to minimize losses, inorganic single-crystalline components (for display LED) and metal structures (interconnects and antenna) must be used.

Thus, the third major task is the heterogeneous integration of components, each created in optimized processes. For example, silicon can be exploited for circuitry, and a direct bandgap III-V material can be utilized for LED-pixels, where silicon is not well-suited. After each component is optimized, they must be electrically connected and mechanically stable in the lens.

The fourth challenge is creating highly-functional and efficient devices that are extremely small. The area of a standard contact lens is about $1\ \mathrm{cm}^2$ with a total thickness of about $200\ \mu\mathrm{m}$. For comparison, the thickness of normal silicon wafers and the smallest surface mount components are between 200 and $500\ \mu\mathrm{m}$.

In this paper, we present our first generation active contact lens containing a wirelessly-powered micro-LED, antenna, and integrated circuit for power harvesting and regulation. First, in Section II, we discuss microfabrication, including the on-lens interconnects and antenna, micro-LEDs, and assembly. Section III describes antenna modeling and design. In Section IV, we present system feasibility analysis using our custom antenna and micro-LED. Section V describes the design of the integrated circuit containing the power harvesting, energy storage and management circuits. System integration is described in Section VI. Section VII presents measurement results, and, lastly, conclusions are presented in Section VIII.

II. Microfabrication

The contact lens substrate provides a platform on which to place and connect various components. To this end, the antenna, electrical interconnects and insulation, soldering pads, and recessed wells to receive complementary-shaped components are fabricated directly on the lens, shown in Fig. 2 and described below [8].

First, a suitable polymer substrate was chosen. The lens substrate must have reasonable chemical and thermal resistance in order to withstand basic microfabrication processing. For example, during photolithography and metal evaporation, temperatures of $75^{\circ}\mathrm{C}$ or greater are common. Additionally, the substrate must maintain its structure upon exposure to common solvents such as acetone and isopropyl alcohol. Another requirement is that the substrate be clear, so as to not obstruct the wearer's vision. Polyethylene terephthalate (PET) is an adequate polymer for this project because it satisfies the aforementioned requirements. Although biocompatibility is a con-

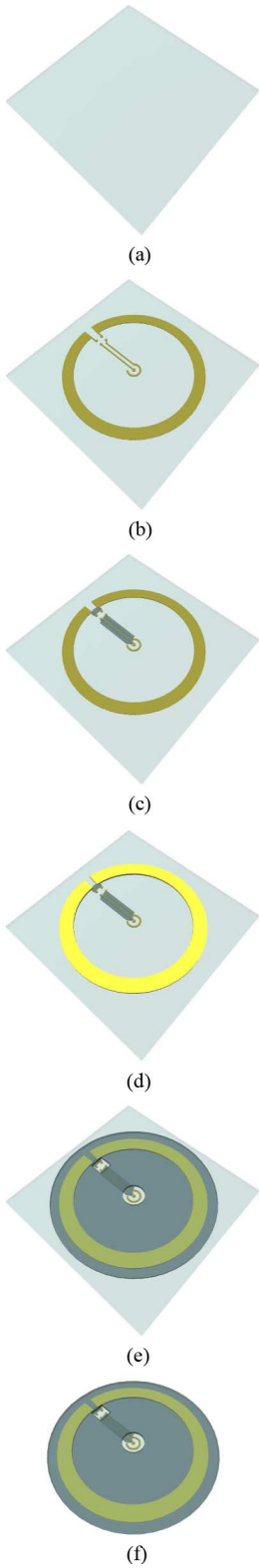

Fig. 2. Process flow of the lens fabrication (a) Start with blank PET wafer (b) Evaporate, lift-off Cr/Ni/Au (c) Spin-on and pattern electrical insulating SU-8 2 (d) Electroplate $5\ \mu\mathrm{m}$ Au antenna (e) Spin-on and pattern thick SU-8 25 for LED well (center) and chip well (upper left) (f) Cut out contacts.

cern, specifically oxygen permeability for long-term wear, the primary focus of this work is to determine system-level feasibility. Therefore, we chose 100 μm thick sheets of PET, laser cut into standard 100 mm wafers, as the lens substrate for our first prototype (Fig. 2(a)).

Next, on-lens electrical interconnects must have very low resistance, must be solderable, and must adhere to PET. Therefore, a metallization of Cr/Ni/Au (20, 80, 400 nm) was used for the electrical interconnects to provide adhesion, solderability, and low resistance, respectively. AZ4620 photoresist (Microchem) was used to pattern the interconnects, and electron-beam evaporation was used to deposit Cr/Ni/Au. Acetone dissolved the photoresist and removed metal in undesired regions (Fig. 2(b)). This metallization also provided an adhesion layer for the antenna. Afterward, a thin, transparent layer of SU-8 2 (Microchem, 1.5 μm) was used as electrical insulation and to restrict solder wetting (Fig. 2(c)).

The antenna must also have very low ohmic losses. Thus, an additional gold layer was electroplated to ensure low resistance. Electroplating was utilized for this task because it was significantly faster and less expensive than alternative solutions. A seed layer of gold was sputtered over the entire wafer and AZ4620 was used to define the antenna. Approximately 5 μm was electroplated, the resist was removed, and the seed layer etched (Fig. 2(d)).

Negative photolithography was used to deposit and pattern permanent SU-8 25 (26 μm) to protect the metal structures and to provide recesses in the surface in which to place components (Fig. 2(e)). Within the recesses are portions of the Cr/Ni/Au metallization that are solderable and complementary to the chip and LED pads. Lastly, the wafer was cut into 1 cm disks using a CO_2 laser cutter (Fig. 2(f)).

A. LED Fabrication

LEDs were fabricated using aluminum gallium arsenide because of its highly efficient emission and proven technology. Fig. 3 shows the process layers and physical dimensions of the custom LED. The active LED layers were grown on an aluminum arsenide sacrificial layer using metal organic chemical vapor deposition, and subsequent processing was performed in-house. The n-type region was etched approximately 1.4 μm into the wafer to reach the p-region. Cr/Ni/Au was deposited and patterned to create n and p-type contacts. Using this approach, both electrical connections are accessible from one side of the LED. The size and shape of the LEDs (circular, 320 μm diameter) were defined using AZ4620, and then the device was etched to reach the sacrificial layer. Finally, the LEDs were released from the wafer using a hydrofluoric acid etch, resulting in thousands of miniscule, free-standing LEDs [9].

The maximum sizes of the micro-LED and other single crystalline components were determined from typical contact lens dimensions. Hard contact lenses are approximately 200 μm thick, 1 cm in diameter, and have a radius of curvature of around 7.8 mm [10]. Single crystalline fabrication is performed on flat surfaces, so the width and thickness of each device must be limited in order to stay within the confines of a lens.

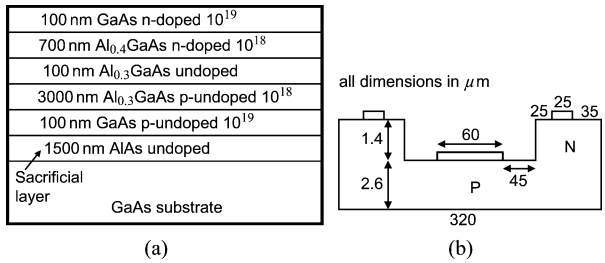

Fig. 3. (a) Material layers of the custom AlGaAs μ-LED. (b) LED dimensions.

Assuming a typical human cornea of 7.8 mm and a base substrate thickness of 100 μm, we determined that all components should have a maximum width of 500 μm with thickness less than 50 μm. The custom IC (Section V) is 250 μm thick but could be thinned in the future.

III. Antenna Design

The primary challenge for antenna design in small systems is to achieve adequate efficiency. Antenna efficiency is strongly influenced by antenna size, and efficiency drops precipitously if the antenna is much smaller than the electromagnetic wavelength [11]. One potential solution to improve the antenna performance with reduced size is to design the system to operate at high frequency. Therefore, we chose the 2.4 GHz ISM frequency band. A loop antenna was determined to be a practical choice to avoid impeding vision. Below we discuss the major challenges in antenna design and characterization.

A. Antenna Design

For a carrier frequency of 2.4 GHz and a maximum loop antenna diameter of 1 cm, the ratio of the circumference of the antenna to the wavelength is about 0.25. Thus the antenna can be loosely approximated as a small loop antenna, and we can estimate its efficiency. The input resistance of an antenna represents dissipation that occurs in ohmic and radiative losses. The radiation resistance of a small loop antenna is given by [11]

$$R_{rad} \approx 32{,}000 \left(\frac{A}{\lambda^2}\right)^2 \tag{1}$$

where A is the area of the loop antenna and λ is the wavelength of the incident RF wave. If the metal thickness is several times the skin depth, and because the RF waves impinge the thin-film antenna only from the top, we can approximate the antenna ohmic losses by

$$R_{ohmic} \approx R_s \left(\frac{2\pi r}{t+w}\right), \text{ with } R_s = \sqrt{\frac{\pi f \mu}{\sigma}} \tag{2}$$

where r, t, and w are loop radius, thickness and width of the antenna trace, respectively, and μ is the permeability of free space. R_s is the surface resistance of the trace and σ is the conductivity of trace metal (gold). Antenna efficiency is defined as

$$\eta = \frac{R_{rad}}{R_{rad} + R_{ohmic}}. \tag{3}$$

Thus, the radiation resistance should be maximized for high efficiency. Moreover, due to the unavailability of high-quality passive components on lens, the antenna impedance must be designed as the complex conjugate of the chip impedance for maximum power transfer. In our design, the chip impedance is about $7\ \Omega + 1.4$ pF, which requires a quality factor (Q) of 6.8 in the impedance of the loop antenna. The choice of chip impedance is discussed in Section V. A circular loop antenna, which is inherently inductive, can tune out the chip capacitance. The real part of antenna impedance, R_{ant}, consists of radiation resistance and ohmic losses. R_{ant}, obtained using EM simulations is $4.2\,\Omega$ which results in a return loss of only 6 dB. At a given frequency, the radiation resistance of the loop antenna is determined by its area alone (1), which in turn is constrained by the size of the lens. Any attempts to improve conjugate matching by increasing real part of antenna impedance implies a higher value of R_{ohmic}. This leads to higher ohmic losses in the antenna degrading its efficiency, indicating an optimal value of R_{ohmic}. Using extensive simulation in ADS Momentum, the optimum antenna impedance was determined to be $4.2\,\Omega + 3\,\mathrm{nH}$ at 2.4 GHz for maximum power transfer under the process constraints. We next describe the antenna modeling and characterization procedure.

B. Modeling and Characterization

The characteristics of antennae are susceptible to the environment, especially near-field ground planes. Thus, the first step was to characterize much larger antennas (diameter $=$ 60 mm, 70 mm, and 80 mm) in air to avoid near-field effects to confirm simulation accuracy and develop a GHz range substrate model. These loop antennae were designed and fabricated using gold traces on a PET substrate. A back-annotated simulation using initial measurement results was used to create an accurate substrate model for our process. Fig. 4(a) captures the substrate model used in our simulations. Fig. 4(b) shows a test antenna matched to 50 Ω for characterization purposes. Fig. 4(c)shows the measured and simulated $|\mathrm{S}_{11}|$ of a 80 mm diameter antenna. Using this model, the simulated performance of a small antenna (5 mm in radius and 0.5 mm in width) and a large antenna (80 mm in radius and 0.5 mm in width) was determined for 2.4 GHz, results of which are shown in Table I. The thickness of our gold metal trace is 5 μm, resulting in a calculated antenna efficiency of 46%.

IV. System Feasibility

In this section, we explore the feasibility of wirelessly powering a micro-LED using a thin film custom antenna on the lens. We derive the constraints on the CMOS rectifier design and impedance matching, and calculate a maximum theoretical distance of operation with a 1 W RF power source.

A. Energy Calculations

In [9], we present custom LEDs, with operating characteristics shown in Fig. 5. The nominal micro-LED turn-on voltage is 3 V with a 400 μW power consumption. If we assume 500 mV of maximum allowable ripple ($V_2 = 3.5$ V and $V_1 = 3.0$ V) on the DC voltage, and a 1 μs ripple period, the size, C, of the storage capacitor is given by

$$\frac{1}{2}CV_2^2 - \frac{1}{2}CV_1^2 = P_{LED} \cdot T \tag{4}$$

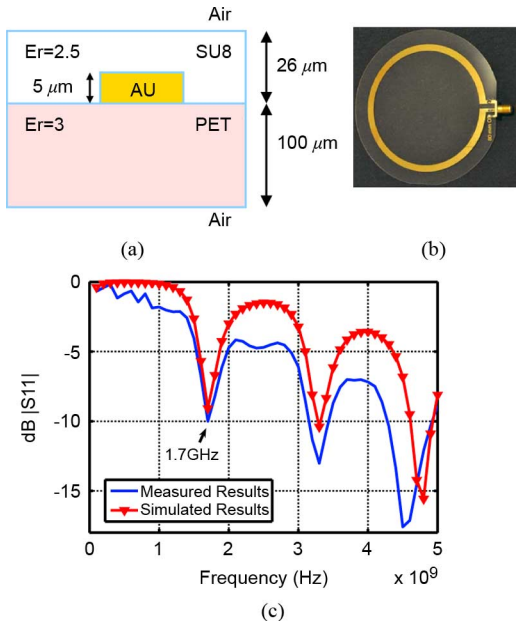

Fig. 4. (a) Substrate model (b) Picture of a larger loop antenna used to confirm simulations and (c) the simulated and the measured results of antenna (diameter $=$ 80 mm and width $=$ 4 mm).

TABLE I
Simulated Antenna Performance

Antenna Parameter	**Small antenna** (r=5 mm, w=0.5 mm)	**Large antenna** (r=80 mm, w=0.5 mm)
Antenna Frequency	2.4 GHz	2.4 GHz
Antenna Gain	-1.81 dB	4.46 dBi
Effective angles	8.06 steradians	4.39 steradians
Directivity	1.93 dB	4.56 dB
Efficiency	46%	97.7%

where P_{LED} is the LED power consumption and T is the ripple period. Equation (4) leads to a 246 pF storage capacitor, which is very large considering the fact that tens of such pixels need to be supplied by the on-chip storage capacitor. The size of storage capacitor and therefore the total stored energy is constrained by the fact that the maximum allowable size of the chip is approximately $500 \times 500\ \mu\mathrm{m}^2$ due to the curvature (≈ 7.8 mm [12]) and thickness ($\approx 200\ \mu$m [10]) of the contact lens. Fortunately, humans cannot perceive light fluctuations above about 60 Hz, and as a consequence duty cycling can be used to make the LED appear continuously activated. We employ 3% duty cycling at 1 MHz frequency, resulting in an average power dissipation of 12 μW per LED. For 500 mV of maximum allowable ripple, this leads to a 7.4 pF storage capacitance value. Given that integrated capacitors of the order of a nF can be realized, 7.4 pF of storage capacitor per pixel is commensurate with our goal of eventually powering tens of such pixels wirelessly.

B. Range Calculations

In order to calculate the maximum range of operation, we need to consider the minimum input power to the antenna and maximum allowed transmit power in 2.4 GHz band. We primarily consider two constraints on this minimum input power: the antenna/rectifier power efficiency, and the input voltage amplitude to the rectifier, which in turn is constrained by the LED turn-on voltage, rectifier threshold, and impedance matching to the antenna.

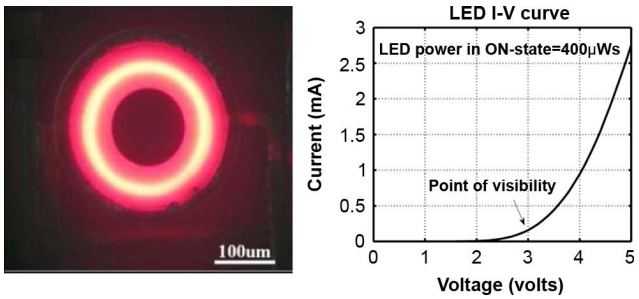

Fig. 5. The lit-up custom LED [8] and its $I - V$ characterstic.

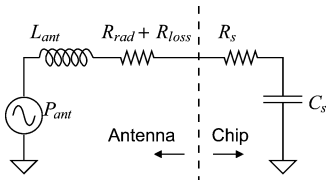

Fig. 6. Conjugate impedance matching between the antenna and the IC.

Using (1)–(3), with $f = 2.4$ GHz, loop radius $r = 5$ mm, trace width $w = 500$ μm, thickness $t = 10$ μm, conductivity $\sigma = 4.52 \times 10^7\ \Omega^{-1}\mathrm{m}^{-1}$, we determine $R_{ohmic} = 0.9\ \Omega$ and $R_{rad} = 0.81\ \Omega$. This leads to theoretical antenna efficiency of 47.3%. However, due to the surface roughness of the electroplated antenna and additional interconnect contact resistance, the effective antenna efficiency could be significantly lower than the theoretical value.

If we assume 10% efficiency of the rectifer and 12 μW LED power consumption, the input power to the chip should be 120 μW. Assuming maximum power transfer and 25% antenna efficiency, the minimum incident power $(P_{Rx,\min})$ on the antenna must be approximately 1 mW (0 dBm).

We now consider the constraint of rectifier input voltage, resulting from necessary output voltage of about 3 V and impedance matching.

Fig. 6 shows the equivalent circuit model of the antenna and the chip. The small loop antenna is approximated as a power source with inductive impedance at 2.4 GHz. In our design, $L_{ant} = 3$ nH, $R_{in} = 7\ \Omega$ and $C_{in} = 1.4$ pF. The quality factor, Q_{in} of the chip input impedance, defined as $1/\omega R_{in} C_{in}$, is approximately 6.8. Assuming conjugate input matching, the available input voltage amplitude V_{in} is given by

$$\frac{P_{ant}}{2} = \frac{V_{in}^2}{2 \cdot R_{in}(1 + Q_{in}^2)} \tag{5}$$

where P_{ant} is the antenna source power as shown in Fig. 6. For rectifier input voltage $V_{in} = 750$ mV, $R_{in} = 7\ \Omega$, $Q = 6.5$, P_{ant} evaluates to be 0.85 mW. Assuming 25% antenna efficiency, this requires 7.4 mW (8.7 dBm) of minimum incident power $P_{Rx,\min}$. This is the deciding constraint on $P_{Rx,\min}$ which we use in the calculations below to evaluate the maximum range of operation.

Assuming line-of-sight communication

$$P_{Rx} = P_{Tx} + G_{Tx} - L_{FS} + G_{Rx} \tag{6}$$

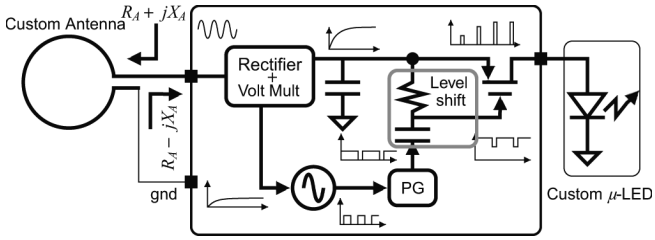

Fig. 7. Architecture of the custom chip.

where P_{Rx} and P_{Tx} are the received and transmit powers (dBm), respectively. G_{Rx} and G_{Tx} are the received and transmit antennae gains (dBi), respectively. L_{FS} represents the free path loss given by [11]

$$L_{FS}(\mathrm{dB}) = 10 \cdot \log_{10}\left(\frac{4\pi df}{c}\right)^2 \tag{7}$$

$$= 20\log_{10}(d) + 20\log_{10}(f) - 147.56. \tag{8}$$

Assuming 10 dBi gain for transmit antenna and an isotropic receive antenna, $P_{Rx} = 8.7$ dBm and 1 W ($P_{Tx} = 30$ dBm) handheld source (maximum transmit power in 2.4 GHz band as allowed by FCC regulations) the range d is 36.5 cm, which satisfies the operational range requirement for our application. However, it must be stated that losses due to suboptimal matching, interface reflections, and absorption in the eye have not been taken into account and could substantially degrade performance. For the bio-safety requirements, we turn to the IEEE standard C95.1, which states that the radiation level for biological safety is approximately $8\ \mathrm{mW/cm^2}$ at 2.4 GHz [13].

V. Radio Power Harvesting IC

Fig. 7 shows the architecture of the CMOS prototype chip containing the power harvesting, storage capacitor (450 pF) and power management circuitry that duty cycles the power-hungry LED pixel.

The difficulty in realizing very small high quality tank circuits directly on the plastic substrate and the extremely small size of the external chip prevents any passive impedance matching circuit for passive voltage gain. This implies a loss of sensitivity of the rectifier. Also the energy storage capacitor must be fully integrated.

Some of the important challenges in making an integrated RF power harvesting system are designing an efficient rectifier, an intelligent, robust power management system, and realizing a high-density on-chip storage capacitor. To avoid junction and oxide breakdown of the transistors in our technology (0.13 μm CMOS), we used the rectifier scheme shown in Fig. 8. We chose a CMOS process that provides low threshold transistors for enhanced rectifier sensitivity. The diodes were realized using PMOS transistors with the body terminal tied to the source in order to eliminate the body effect.

The optimal number of stages in the multiplying rectifier was determined by considering the trade-off between power efficiency, output voltage, input impedance for matching, and the micro-LED load (capacitor charging time). For maximum energy storage on the capacitor, the DC voltage must be maximized under the breakdown voltage constraint (10 V). This

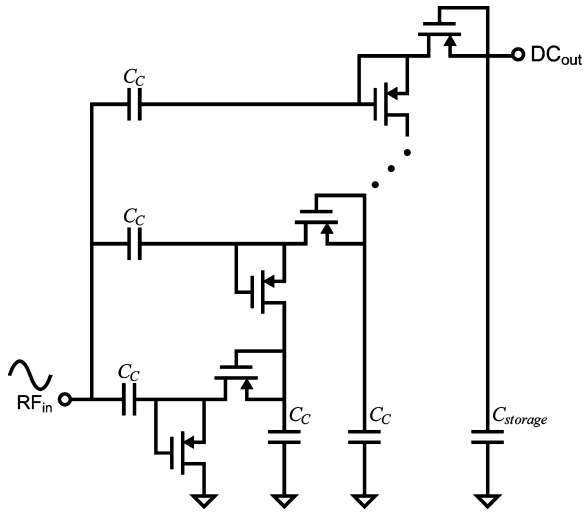

Fig. 8. Eight-stage rectifier design using low-V_t PMOS devices. $C_c = 1$ pF and $C_{\text{storage}} = 450$ pF.

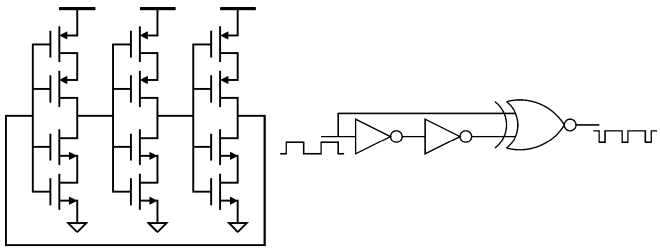

Fig. 9. (a) Low leakage ring oscillator using high-V_t stacked transistors. (b) Frequency doubling pulse generation circuit.

breakdown constraint comes from the voltage breakdown of the high density Metal-Insulator-Metal (MIM) capacitors. However, the large number of stages required for achieving this high voltage leads to increased capacitor charging time, degraded quality factor of the input impedance, and unreasonable values for the antenna impedance matching [14].

Another important aspect of the rectifier design is the choice of coupling capacitor (C_c). It should be much larger than the parasitic capacitance of the MOS diodes, but should be small enough to facilitate input matching and higher quality factor of the input impedance of the chip (for passive voltage gain). For our application, 1 pF was found to be a good compromise. For an on-lens display application using our custom LEDs, the optimal number of stages was found to be eight. This provides approximately $8 \cdot (V_{RF} - V_{th}) \approx 3.6$ V of DC output for 750 mV of RF input and a 300 mV threshold voltage (V_{th}).

As described in Section IV, the LED must be duty cycled to enable operation using RF power. The duty-cycling circuitry activates the LED for approximately 3% of the time by modulating the 3.3 V PMOS switch. It consists of a ring oscillator, pulse generator and a passive level shifter circuit (Fig. 7). The ring oscillator shown in Fig. 9(a) derives its power supply $(\sim 1$ V) from the second stage of the cascaded rectifier. Each inverter in the 3-stage oscillator uses stacked high-V_t devices for low leakage and low-power operation (~ 500 nW at 1 MHz).

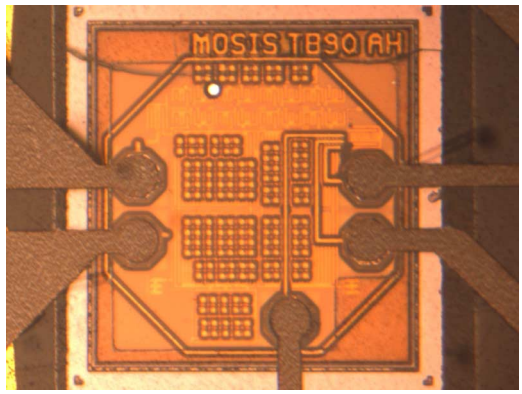

Fig. 10. A flip-chip assembled CMOS die on the transparent contact lens substrate.

The frequency doubling pulse generation circuit shown in Fig. 9 generates an active low pulse at each transition of the oscillator output of duration approximately $0.015/f$, where f is the frequency of the ring oscillator. This means that the pulse generator effectively generates active low pulses with a 3% duty cycle at a frequency $2f$. The level shifter circuit uses the rectifier output $(\sim 1$ V) to upconvert the 1 V active-low pulses with active-high and active-low being 3.5 and 2.5 V, respectively.

VI. System Integration

After the substrate, antenna, electrical interconnects, and various independent components were fabricated, they were integrated to form a complete system. To this end, a low temperature solder (60° C, Indium Co.) was melted and pipetted over the contact lens templates (Fig. 2(f)) to wet the exposed gold within the SU-8 recesses. The pads of power harvesting and regulation circuit, discussed in Section V, were electrolessly plated with nickel and gold to create a solderable surface. After plating, these pads were independently coated with solder because the surface roughness made wetting difficult. LED pads were sufficiently smooth, and did not require independent solder coating. In a fluidic environment, components were placed using a micro-positioner or pipette, and the solder was reflowed to connect the substrate to the components [15]. Capillary forces of the mold solder acted to very accurately align the components and correct for misplacement (Fig. 10). Lastly, the planar lens with components attached was placed and pressed in a heated aluminum mold $(180°\text{C})$ to obtain the correct curvature. After molding, the lens edges were polished, and several micrometers of biocompatible parylene were conformally deposited over the entire device at room temperature.

VII. Measurement Results

Fig. 11 shows the measured efficiency of the rectifier system while powering the LED at 3 V. At low input power, the efficiency drops due to leakage in the rectifier, while at high input power, ohmic losses in the rectifier degrade the efficiency. The peak efficiency of 10% compares favorably with the start-of-the-art value for 2.4 GHz [16]. Rectifier DC output is shown in Fig. 12 for 2.4 GHz input signal.

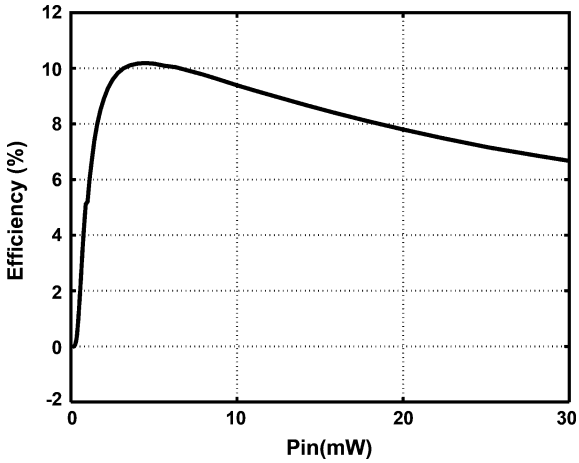

Fig. 11. Measured efficiency of the power harvesting system.

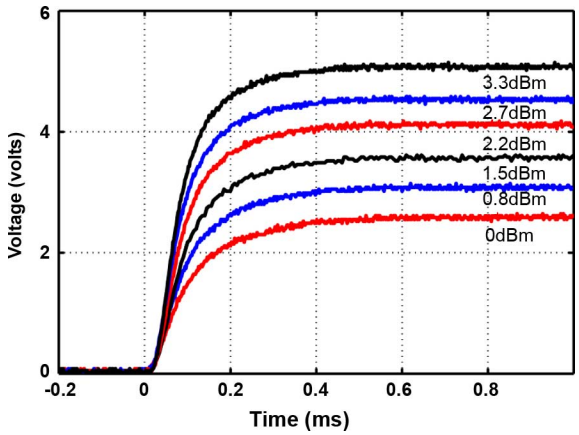

Fig. 12. Rectifier output voltage with 2.4 GHz input under no-load condition.

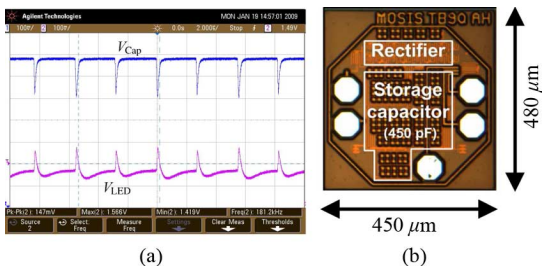

Fig. 13. (a) The level-shifted duty-cycled pulse and the voltage pulses applied to the μ-LED. (b) Chip micrograph.

Fig. 13(a) captures the waveforms, V_{LED} and $V_{Level-Shifter}$ at the drain and gate terminals of the PMOS duty-cycle control switch, respectively. Fig. 13(b) shows the chip micrograph $(450 \times 480\ \mu\text{m}^2)$.

The total power dissipation of the system is $124.9\ \mu$W while delivering $12\ \mu$W of average power to the display LED. The measured power breakdown of the individual building blocks is not available as we do not have their supply nodes available for current measurement. Due to size constraint on the IC, we could not accommodate more output pads for characterization.

Fig. 14 shows the pictures of the contact lens assembly and wirelessly lit lens using a $+25$ dBm RF source.

Fig. 14. Unlit and wirelessly lit active lens assembly.

TABLE II
PERFORMANCE COMPARISON.

	This work	**[17]**	**[18]**	**[19]**
Carrier Frequency	2.4 GHz	900 MHz	900 MHz	900 MHz
System Power	124.9 μW	18.4 μW	12 μW	5.1 μW
Transducer	Display LED	Temp. sensor	Temp. sensor	Temp., photo sensor
External components	Zero	Matching net., storage cap.	Not available	Not available
Process	0.13 μm	0.13 μm	0.18 μm	0.18 μm
Chip Area	0.2 mm^2	2 mm^2	1.1 mm^2	0.4 mm^2*

*excluding pads

Using a 2 GHz dipole antenna at the RF source, we have demonstrated an LED turn-on range of approximately 10 cm using a $+25$ dBm RF source. Therefore, we are operating close to the far field of the dipole antenna.

Table II presents the comparison of this work with recent work on RF-powered sensor systems. Higher frequency of operation, very small antenna (≈ 1 cm in diameter) and die size, and absence of any off-chip components are unique features of this work that lead to lower system efficiency than what is possible in meso-scale implementations.

With improved matching and antenna efficiency (with lower surface roughness) we expect a longer operational distance. In addition, we expect to improve LED efficiency significantly, which would greatly decrease system power requirements. Going forward, we plan to conduct in-vivo testing on a lens incorporating multi-pixel display, bio-sensors (temperature, intra-ocular pressure and glucose) and full-fledged bio-telemetry.

VIII. CONCLUSION

We have taken the first steps toward creating an active contact lens. We have demonstrated that a small loop antenna connected through a power harvesting IC can power a micro-LED on a transparent substrate. We verify the operational distance to be 10 cm while satisfying biological radiation safety criteria. Through optimization of the antenna and impedance matching, we hope to create a system with a multiple LED pixels and sensing capability with operating distance over several tens of centimeters.

REFERENCES

[1] B. Parviz, "For your eye only," *IEEE Spectrum*, vol. 46, no. 9, pp. 36–41, Sep. 2009.
[2] A. Shum, M. Cowen, I. Lähdesmäki, A. Lingley, B. Otis, and B. Parviz, "Functional modular contact lens," in *Proc. SPIE*, 2009, vol. 7397, no. Biosensing II (2009), pp. 73970K/1–73970K/8.

[3] S. S. Lane and B. D. Kuppermann, "The implantable miniature telescope for macular degeneration," *Current Opin. Ophthalmol.*, pp. 94–98, 2006.
[4] M. Leonardi, P. Leuenberger, D. Bertrand, A. Bertsch, and P. Renaud, "A soft contact lens with a MEMS strain gage embedded for intraocular pressure monitoring," in *Proc. Int. Conf. Transducers, Solid-State Sensors, Actuators and Microsystems*, 2003, vol. 2, pp. 1043–1046.
[5] K. Stangel, S. Kolnsberg, D. Hammerschmidt, B. J. Hosticka, H. K. Trieu, and W. Mokwa, "A programmable intraocular CMOS pressure sensor system implant," *IEEE J. Solid-State Circuits*, vol. 36, no. 7, pp. 1094–1100, Jul. 2001.
[6] H. Cong and T. Pan, "Microfabrication of conductive PDMS on flexible substrates for biomedical applications," in *Proc. IEEE Int. Conf. Nano/Micro Engineered and Molecular Systems*, 2009, pp. 731–734.
[7] D. Puttjer, F. Pramassing, R. Buss, and D. Jager, "LED-Based micro display for an intraocular vision aid (IOVA)," in *Proc. 23rd Int. Conf. IEEE Engineering in Medicine and Biology Soc.*, 2001, vol. 4, pp. 3436–3439.
[8] H. Ho, E. Saeedi, S. S. Kim, T. T. Shen, and B. A. Parviz, "Contact lens with integrated inorganic semiconductor devices," in *Proc. IEEE Int. Conf. MEMS*, Jan. 2008, pp. 403–406.
[9] E. Saeedi, S. S. Kim, and B. A. Parviz, "Self-assembled inorganic micro-display on plastic," in *Proc. IEEE Int. Conf. MEMS*, Jan. 2007, pp. 755–758.
[10] A. Phillips *et al., Contact Lenses*, Fifth ed. New York: Elsevier, 2007.
[11] W. L. Stutzman and G. A. Thiele, *Antenna Theory and Design*. New York: Wiley.
[12] H. Y. Patel, D. V. Patel, and C. N. J. McGhee, "Identifying relationships between tomography-derived corneal thickness, curvature, and diameter," *Eye*, vol. 23, pp. 270–278, Feb. 2008.
[13] *IEEE Standard*, IEEE Std. C95.1-2005.
[14] T. Le, K. Mayaram, and T. Fiez, "Efficient far-field radio frequency energy harvesting for passively powered sensor networks," *IEEE J. Solid State Circuits*, vol. 43, no. 5, pp. 1287–1302, May 2008.
[15] S. A. Stauth and B. A. Parviz, "Self-assembled single crystal silicon circuits on plastic," *Proc. Nat. Acad. Sciences*, vol. 103, no. 38, pp. 13922–13927, Sep. 2006.
[16] K.-H. Chen, J.-H. Lu, and S.-I. Liu, "A 2.4 GHz efficiency-enhanced rectifier for wireless telemetry," in *Proc. IEEE Custom Integrated Circuits Conf.*, 2007, pp. 555–558.
[17] D. Yeager, F. Zhang, A. Zarrasvand, and B. P. Otis, "A $9.2\ \mu\mathrm{A}$ gen 2 compatible UHF RFID sensing tag with $-12\ \mathrm{dBm}$ sensitivity and $1.25\ \mu\mathrm{V_{rms}}$ input-referred noise floor," in *Proc. IEEE Int. Solid-State Circuits Conf.*, 2010, pp. 52–53.
[18] J. Yin, J. Yi, M. K. Law, Y. Ling, M. C. Lee, K. P. Ng, B. Gao, H. C. Luong, A. Bermak, M. Chan, W.-H. Ki, C.-Y. Tsui, and M. Yuen, "A system-on-chip EPC Gen-2 passive UHF RFID tag with embedded temperature sensor," in *Proc. IEEE Int. Solid-State Circuits Conf.*, 2010, pp. 308–309.
[19] N. Cho, S.-J. Song, S. Kim, S. Kim, and H.-J. Yoo, "A 5.1 μW UHF RFID tag chip integrated with sensors for wireless environmental monitoring," *Proc. IEEE ESSCIRC*, pp. 279–282, 2005.

Jagdish Pandey (S'07) received the B.Tech. degree from the Indian Institute of Technology, Madras, in 2003, the M.Sc. degree from the Indian Institute of Science, Bangalore, in 2007, and is currently pursuing the Ph.D. degree at the University of Washington, Seattle.

He was an RFIC Design Intern at Broadcom Corp. in 2010. His research interests are in the area of energy-efficient communication circuits.

Yu-Te Liao (S'05) received the B.S. degree in electrical engineering from National Cheng Kung University, Tainan, Taiwan, in 2003, the M.S. degree in electronics engineering from National Taiwan University, Taipei, Taiwan, in 2005, and is currently pursuing the Ph.D. degree at the University of Washington, Seattle.

His research interests include low-power radio-frequency integrated circuits, integrated sensors, and biomedical circuits and systems.

Andrew Lingley received the B.S. degree in electrical engineering from Montana State University, Bozeman, in 2007 and is currently pursuing the Ph.D. degree at the University of Washington, Seattle.

He interned at the Pacific Northwest National Laboratory during summers 2005 through 2007. His current research focuses on developing a contact lens with embedded electronics and optoelectronics. His research interests include using solar energy to power chemical sensors and microfabrication on nonstandard substrates.

Ramin Mirjalili received the B.Sc. and M.Sc. degrees from Sharif University of Technology, Tehran, Iran, and is currently pursuing the Ph.D. degree with a focus on the integration of electronics and optics on bionic contact lens at the University of Washington, Seattle.

He studied electrical and petroleum engineering in his undergraduate studies and continued his studies in electronics with a focus on microelectronics circuitry and biosensors.

Babak Parviz was a Device Designer and a Product Manager working on integrated photonics with Nanovation Technologies, Inc., from 2000 to 2001. He joined the Department of Chemistry and Chemical Biology at Harvard University, Cambridge, MA, as a Postdoctoral Research Fellow in 2001. At Harvard, he was involved in research on developing novel nanofabrication technologies, self-assembled systems, low-cost biosensing, and using organics for electronics and microelectromechanical systems. He joined the Electrical Engineering Department, University of Washington, Seattle, as a faculty member in 2003. Currently, he is the Associate Director of the Micro-scale Life Sciences Center at the University of Washington.

Dr. Parviz is a founding member of the American Academy of Nanomedicine and a member of the American Association for the Advancement of Science, American Chemical Society, Association for Research in Vision and Ophthalmology, and Sigma Xi.

Brian P. Otis (S'96–M'05–SM'10) received the B.S. degree in electrical engineering from the University of Washington, Seattle, and the M.S. and Ph.D. degrees in electrical engineering from the University of California, Berkeley.

He joined the faculty of the University of Washington as Assistant Professor of Electrical Engineering in 2005. His primary research interests are ultra-low-power radio-frequency integrated-circuit design and bioelectrical interface circuits and systems. He previously held positions at Intel Corp. and Agilent Technologies. He served as an Associate Editor of the IEEE TRANSACTIONS ON CIRCUITS AND SYSTEMS—PART II: EXPRESS BRIEFS.

Dr. Otis received the U.C. Berkeley Seven Rosen Funds Award for innovation in 2003, was co-recipient of the 2002 ISSCC Jack Raper Award for an Outstanding Technology Directions Paper, and recipient of the National Science Foundation CAREER award in 2009.